Effects of Oxygen Plasma Treatment on Fermi-Level Pinning and Tunneling at the Metal–Semiconductor Interface of WSe$_2$ FETs

Kwangro Lee, Tien Dat Ngo, Sungwon Lee, Hoseong Shin, Min Sup Choi, James Hone, and Won Jong Yoo*

Recently, 2D materials have been intensively investigated for their novel nano-electronic applications; among these materials, tungsten diselenide (WSe$_2$) is attracting substantial research interest due to its high mobility, sizable bandgap, and ambipolar characteristics. However, Fermi-level pinning (FLP) at the metal–semiconductor contact is a critical issue preventing further integration of WSe$_2$ to complementary metal–oxide–semiconductor (CMOS) technology. In this study, a facile doping method of oxygen (O$_2$) plasma treatment and an aging effect to overcome the FLP of WSe$_2$ field-effect transistors (FETs) are utilized. After aging, a reduction is observed in FLP on oxidized WSe$_2$ FETs, along with a decrease in pinning factor (S) for holes from −0.06 to −0.36. Further, the field-effect mobility of high- (Pd) and low- (In) work-function contacted WSe$_2$ devices indicates the presence of more improvement in high-work-function metal-contacted p-type WSe$_2$ FETs, which further strengthens the Fermi level de-pinning behavior attributed to the O$_2$ plasma and aging processes. The existence of different tunneling behaviors of Pd and In devices also confirms the effect of O$_2$ plasma doping into WSe$_2$ FETs. Ultimately, this work demonstrates a simple and efficient method for achieving the de-pinning of Fermi-levels and modulating FLP of 2D FETs.

1. Introduction

Transition metal dichalcogenides (TMDs) have emerged as next-generation semiconducting materials that have attracted substantial attention in various fields, and extensive research examining these TMDs is currently underway due to their potential for use in future electronic, optoelectronic, and quantum devices, which is attributed to their unique 2D structure,[1,2] wherein two adjacent layers are stacked by the weak van der Waals (vdW) force due to their potential for realizing atomic-scale stack devices without interference arising from dangling bond free surface.[3–7] Since they can be stacked to form heterostructures with other materials, TMDs have been shown to exhibit diverse functionalities realized from 2D heterostructures, along with additional advantages such as a direct bandgap for photonic applications and reconfigurable semiconductor polarity.[8–14]

Among the TMDs, tungsten diselenide (WSe$_2$) can be doped through various methods developed for 2D materials, such as oxygen (O$_2$) plasma or UV–ozone (O$_3$) treatment[10,15] and surface chemical dopants.[12] WSe$_2$ after O$_2$ plasma treatment has been reported to show a carrier mobility exceeding 200 cm^2 V^{-1} s^{-1},[13] which is different from its metallic behavior immediately after O$_2$ plasma treatment.[14] Here, it is expected that air exposure will convert the metallic state to the semiconducting state due to the change in its surface.[16] That is, we expect that the incorporation of carbon impurities between WSe$_2$ and tungsten oxide (WO$_x$) or the desorption of oxygen atoms will play a key role in altering the surface of WO$_x$, thus leading to a p-type semiconductor over time.[16]

Fermi-level pinning (FLP) occurs at the metal–semiconductor (MS) interface in which the Schottky barriers do not match with the work function differences between 2D material and contacting metal. The FLP originates from the fixed Fermi level of the semiconductor at the charge neutral level (CNL), thus affecting the transport of electrons and holes across the junction and the electrical contacts of the device.[17,18] There have been various studies aiming to overcome the FLP by de-pinning the fixed Fermi-level, e.g., contact doping, introduction of an additional interlayer at the junction,[19] and 1D edge contacts.[20,21]

K. Lee, T. D. Ngo, S. Lee, H. Shin, W. J. Yoo
Department of Nano Science and Technology
SKKU Advanced Institute of Nanotechnology (SAINT)
Sungkyunkwan University
2066 Seobu-ro, Jangan-gu, Suwon, Gyeonggi-do 16419, Republic of Korea
E-mail: yoowj@skku.edu
M. S. Choi
Department of Materials Science and Engineering
Chungnam National University
99, Daehak-ro, Yuseong-gu, Daejeon 34134, Republic of Korea
J. Hone
Department of Mechanical Engineering
Columbia University
New York, NY 10027, USA

The ORCID identification number(s) for the author(s) of this article can be found under https://doi.org/10.1002/aelm.202200955.

In this work, we administered O_2 plasma treatment onto the intrinsic WSe_2 after metallization for the purpose of investigating the FLP and contact properties at the MS junction. Hall-bar structured devices with precisely defined channel length and channel width were fabricated and measured by the four-point probe (4PP) method to separately extract the channel and contact resistances. During aging, the devices were stored in vacuum at room temperature for a certain period of time for further testing. The aged devices revealed a semiconducting behavior with a clear off-current, unlike the devices immediately after the O_2 plasma treatment, which showed a metallic behavior. We also explored the effects of FLP on the contact and tunneling properties across the MS junction in the O_2-plasma-treated and aged WSe_2 devices using various metal contacts.

2. Results and Discussion

2.1. O_2 Plasma Treatment and Aging of WSe_2 FET Devices

Figure 1a shows the key processing steps of the plasma-treated and subsequently aged WSe_2 field effect transistors (FETs). The device fabrication was conducted by mechanically exfoliating WSe_2 on thin and flat poly(dimethylsiloxane) (PDMS) and transferring it onto a SiO_2 substrate that was cleansed by acetone and isopropyl alcohol (IPA). WSe_2 was exfoliated on PDMS rather than SiO_2 substrate to avoid incorporating processing residues or other scattered flakes. After transferring the WSe_2 onto a silicon substrate, it was patterned for 4PP measurements

via electron beam lithography (EBL) and subsequent plasma etching. Then, different contact metals covered by Au were deposited onto each flake with surface contact. Figure 1b shows a schematic diagram of the fabricated WSe_2 devices for the 4PP measurement setup, and Figure 1c shows an optical image of the fabricated Pd- and In-contacted devices from the same flake with a 10 µm scale bar. The electrical properties of the devices are measured separately to investigate the contact and channel-aged WSe_2 FETs. Otherwise, high- and low-work-function metals are used to examine the modification of MS contact attributed to surface charge transfer doping of the channel of WSe_2 FETs by O_2 plasma treatment. As shown in **Figure 2**a, the pristine state of both high (Pd) and low (In) work function contacting WSe_2 FETs shows n-type dominant ambipolar semiconducting behavior, which is a typical FLP behavior of WSe_2 FETs.[12,22] Moreover, the overall resistance of the devices is high (Figure 2b), thus necessitating an effective doping method. Here, we used O_2 plasma treatment, which is responsible for the p-type metallic behavior without the off-current state of WSe_2 FETs for both metals. Due to the formation of an amorphous WO_x layer on top of the WSe_2, we observed a significant improvement in the resistance of the device after the aging process. In contrast to the pristine state, the performance of the Pd-WSe_2 device after oxidation and aging process is five times better than that of the In-WSe_2 device, which is consistent with the band alignment results of metal and WSe_2. This is evidence of the Fermi-level de-pinning behavior of the WSe_2 device via charge transfer doping.[12,23] However, it is difficult to quantitively evaluate how much the Fermi level of
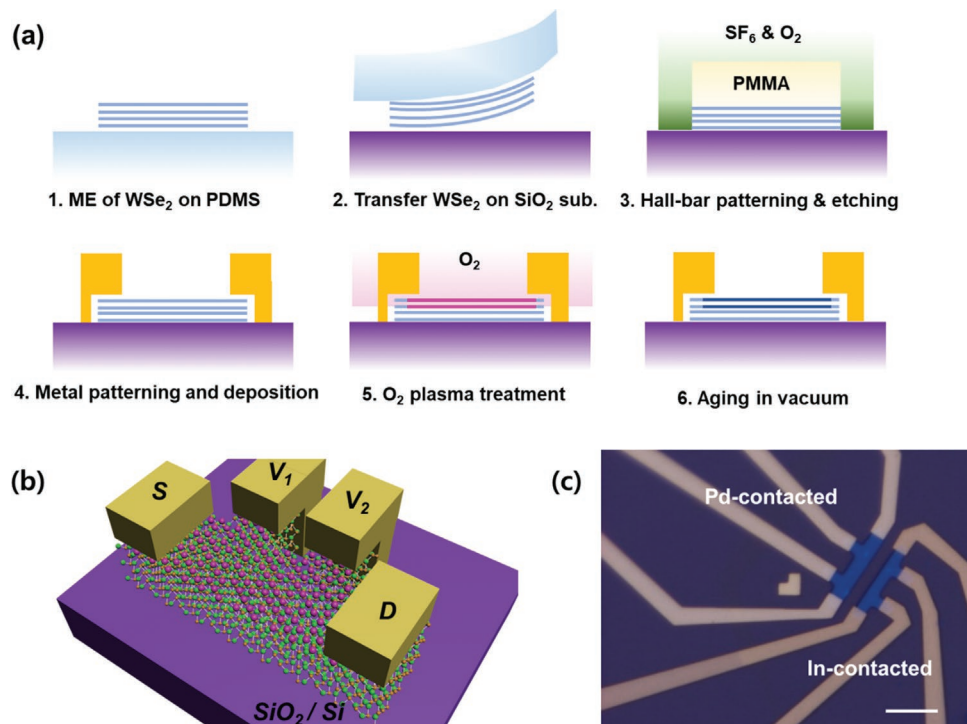
Figure 1. a) The fabrication process of a WSe_2 FET device. The Hall-bar pattern was formed by performing EBL and plasma etching. Each of the contact metals covered by Au was deposited onto the WSe_2. The device was treated with O_2 plasma onto the whole surface, after which it was vacuum-aged. b) Schematic diagram of O_2-plasma-treated WSe_2. c) Optical image of the fabricated Pd- and In-contacted devices; scale bar: 10 µm.
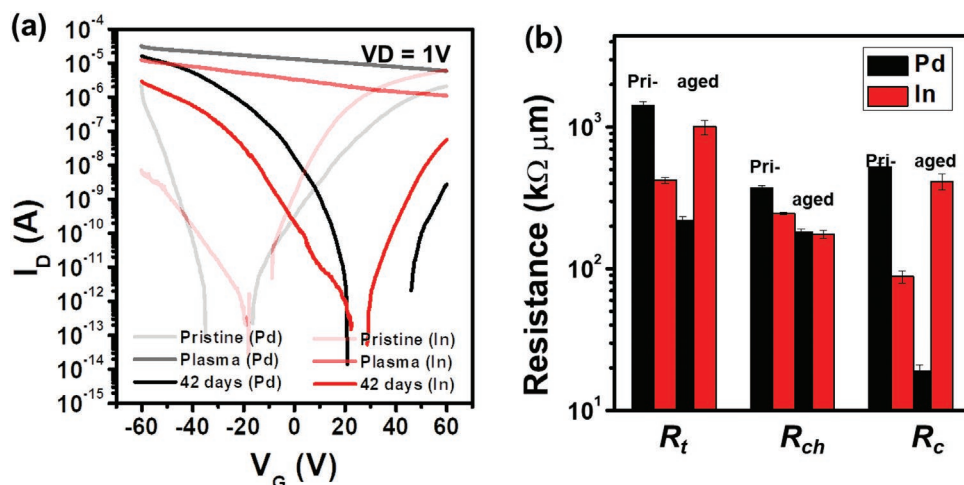
Figure 2. Electrical properties of pristine and aged doped WSe_2 FET devices for Pd- and In-contacts. a) The aging effect over different periods from pristine to more than a month. b) A comparison of the resistance before and after the doping and aging processes.

WSe_2 is de-pinned without off-state of the device. Therefore, recovery of the off-state for heavily p-doped WSe_2 immediately after the O_2 plasma treatment is desired for determining the FLP effect on our device. The simplest way to obtain the aforementioned behavior is natural aging of an oxidized WSe_2 device, as shown in Figure 2a. After 42 days of preservation in a vacuum desiccator, the transfer curve of the oxidized WSe_2 FETs demonstrates semiconducting behavior, as we expected for both types of metal. The aging mechanism of oxidized WSe_2 FETs is further discussed in the following.

Figure 2a shows the transfer curves of WSe_2 FETs with O_2 plasma doping obtained from different aging processes. Immediately following the O_2 plasma treatment, the metallic property was observed without off-state. Thus, to fulfill our purpose of investigating the Schottky barrier height (SBH) and logic circuit application of oxidized WSe_2 FETs, we intentionally perform a subsequent aging process to recover the off state of the degenerate doped WSe_2 FETs. The degradation of oxidized WSe_2 can be attributed to carbon contamination and the adsorption of O_2 and H_2O molecules from air at the WO_x surface, which harms the device performance.[16,24] Moreover, doping of O_2 plasma to WSe_2 is originated to the dangling bonds of WSe_2. Meanwhile, a noticeable amount of oxygen atoms is physically absorbed on the surface of WSe_2 while performing O_2 plasma treatment.[25,26] Therefore, the aforementioned oxygen atoms can easily desorb from the WSe_2 surface to restore the off state of a degenerate p-type WSe_2 after the self-aging process. Thus, samples were stored in a vacuum desiccator during aging for the purpose of avoiding degradation other than the self-desorption of oxygen atoms.

To comprehensively probe the contact properties of the WSe_2 device during fabrication process, we performed 4PP measurement. Figure 2b shows the resistances of the device measured by carrying out 4PP at pristine state and after aging, which consists of total resistance (R_t), channel resistance (R_{ch}), and contact resistance (R_c). The channel resistance values of both Pd- and In-contacted devices show slight improvements compared to the pristine state after a long aging period. Regarding contact resistance, R_c of the Pd-contacted device is much higher than that of the In-contacted device at $V_G = 60$ V. Meanwhile, for aged

devices with p-type behavior, we observed an opposite trend, which is a relatively decreased contact resistance for the high-work-function metal (Pd- contacted device) with respect to the low-work-function metal (In-contacted device) at $V_G = -60$ V. Moreover, after aging, Pd- and Au-contacted devices also show a quasi-Ohmic contact behavior that is in contrast to the Schottky contacts of the In- and Ti-contacted devices (See Figure S1, Supporting Information). In fact, this result is controversial as it relates to the physical properties of the metal–WSe_2 interface. With In contact, the metal–semiconductor interface shows an ultra-clean surface that is free from defects.[27,28] For Pd contact, the formation of PdO is often observed, which limits the performance of a Pd-contacted device.[29] Thus, the change in the trend of R_c and the output characteristics should be explained by another mechanism. Although O_2 plasma treatment was not performed at the interface between WSe_2 and metal directly underneath a metal, another study has shown that channel area doping also affects the metal–WSe_2 contact properties.[12,23,30] We further investigated the carrier concentrations of our Pd and In contact devices for the pristine, immediately after plasma treatment, and aged statuses by obtaining the transfer curves shown in Figure 2a. In the case of Pd, the carrier concentrations were calculated as 1.13×10^9, 3.60×10^{12}, and 1.39×10^{12} cm^{-2} for pristine, immediately after plasma, and aged, respectively. In the case of In, the respective values were calculated as 1.38×10^{11}, 3.18×10^{12}, and 5.93×10^{11} cm^{-2}. Both hole concentrations of Pd and In contact devices increased after the O_2 plasma treatment and decreased after aging. It can clearly be seen that the hole concentration increased after aging, although the hole concentration changes in In contact are smaller than those in Pd contact (see Figure S2, Supporting Information). The surface profile of the O_2-plasma-treated WSe_2 flakes was also confirmed by Raman spectroscopy and atomic force microscopy, as shown in Figure S3 (Supporting Information). The frequency difference between the E_{2g} and A_{1g} vibration modes shows a slight change before and after the O_2 plasma treatment and aging process. The thickness of the plasma-treated WSe_2 flakes also changed with time. Based on the change observed from Raman spectroscopy results, we conclude that the physical properties
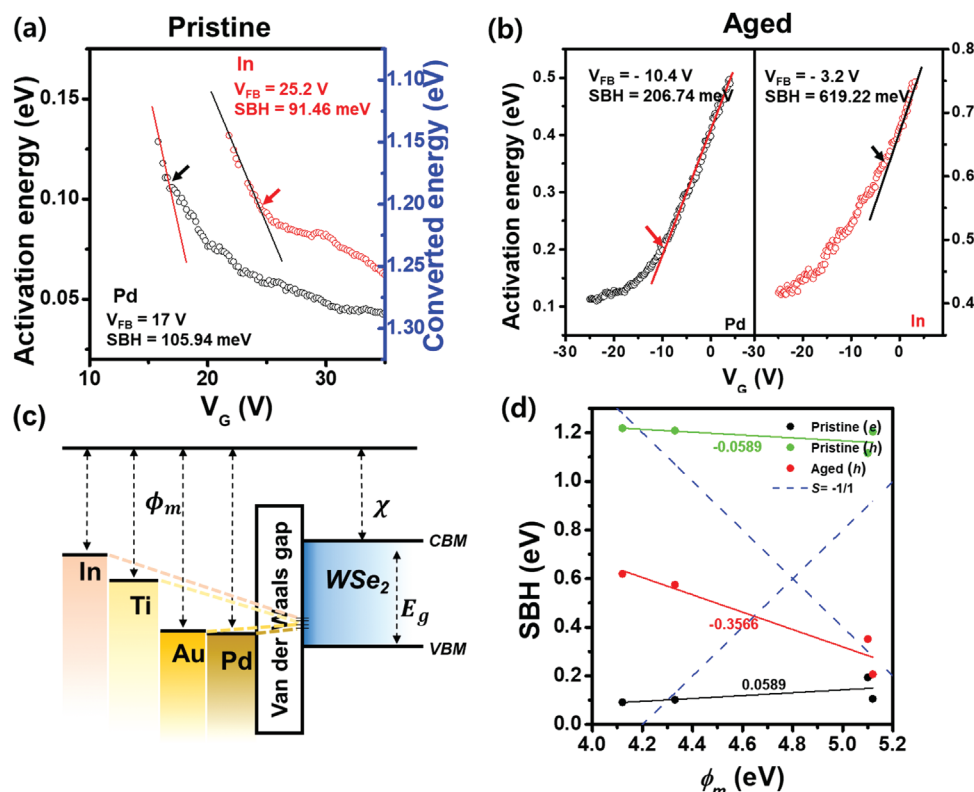
Figure 3. Comparison of SBH before and after the aging process. a,b) SBH extracted from Pd- and In-contacted devices before and after the aging process, respectively. c) Simplified explanation of FLP. d) The extracted pinning factor (S) for our devices with four metal contacts and with the pinning factors converted from electron to hole.

of WSe$_2$ lattice continuously changed while proceeding with aging in vacuum.

To further confirm the mechanism responsible for the transition of the contact properties of WSe$_2$ after oxidation and aging processes, we investigate the SBH of our device as described in the next section.

2.2. Schottky Barrier Height and Fermi-Level Pinning

FLP was revealed by extracting the SBH. The SBH for a hole can be given as

$$\phi_B = \chi + E_g - \phi_m \tag{1}$$

where ϕ_B is the SBH, ϕ_m is the work function of the metal, E_g is the bandgap energy, and χ is the electron affinity of the semiconductor, which is 4.06 eV (see Figure S4 of the Supporting Information for the conversion of SBHs).

In the case of the Schottky–Mott limit, the pinning factor (S) is equal to −1 for hole. In general, FLP at the MS junction results from the band alignment of different material junctions. In this case, the barrier height is expected to be adjusted according to the work function of contact metals. However, as shown in **Figure 3**c, the Fermi level is fixed at a certain state for most MS junctions regardless of the work function of a contact metal used, thus showing that Schottky contact is unavoidable.

Equation (1), following the Schottky–Mott rule, can be rewritten by applying the S and the CNL, as shown in the following Equation (2). The SBH for p-type semiconductors decreases as the work function of metal increases.[22]

$$\phi_B = S\left(\phi_m - \phi_{CNL}\right) + \left(\chi + E_g - \phi_{CNL}\right) = S\phi_m + b \tag{2}$$

where $S = \dfrac{d\phi_B}{d\phi_m}$.

S has a negative value for SBH of p-type semiconductors, unlike SBH of n-type semiconductors. That is, for p-type semiconductors, the closer the pinning factor is to −1, the stronger the de-pinning, while the closer the pinning factor is to 0, the stronger the pinning.

To extract the SBH values, we adopted the following thermionic emission equations.[32–34]

$$I_{2D} = WA_{2D}^* T^{3/2} \exp\left(-\frac{q\phi_B}{kT}\right)\exp\left(\frac{qV_D}{kT}\right), \quad A_{2D}^* = \frac{q\sqrt{8\pi m^* k^3}}{h^2} \tag{3}$$

$$\phi_B = k\left[\frac{\Delta \ln\left(I_D/T^{1.5}\right)}{\Delta T^{-1}}\right] \tag{4}$$

Here, k is the Boltzmann constant with the unit of eV, I_D is the drain current of the device, T is the temperature (K), A_{2D}^* is the modified Richardson constant, and W is the width of the transport channel. The SBH can be derived by taking a derivative of drain current at various temperatures.

Table 1. Extracted Schottky barrier heights for pristine and aged WSe$_2$ devices.

Metal	ϕ_m [eV][31]	ϕ_{Bn} [meV]	Converted ϕ_{Bp} [meV][22]	Aged ϕ_{Bp} [meV]
In	4.12	91.46	1218.54	619.22
Ti	4.33	101.57	1208.43	574.63
Au	5.1	193.91	1116.09	351.77
Pd	5.12	105.94	1204.06	206.74

To extract the SBHs of our devices, we first investigated the band alignment of WSe$_2$ to reveal the reduced FLP. We adopted the bandgap energy and affinity of 1.31 and 4.06 eV, respectively, for WSe$_2$.[35] We then made a calculation using Equation (4) for various gate voltages. From our results, SBH for the electron of the pristine WSe$_2$ was first calculated from transfer curves with varied temperatures, and the values were extracted as 106 meV for Pd and 91 meV for In, as shown in Figure 3a. Those SBHs for the electron were then converted to SBHs for hole by subtracting the bandgap energies of WSe$_2$, which are 1204 meV for Pd and 1218 meV for In for hole SBH. The converted SBHs are the values obtained by converting the formula S4 in Supporting Information in the pristine state from electron SBH to hole SBH. For the Pd-contacted WSe$_2$ in the pristine state, since we obtained a transfer curve with a stronger n-type, we interpreted it as n-type, and calculated it based on electron when calculating SBH by considering it as the main carrier. Note that the value was used to show that the FLP was reduced after the aging process and became smaller. The SBHs for aged devices were extracted as 207 meV for Pd and 619 meV for In, as shown in Figure 3b. Moreover, we investigated and extracted the SBH for Ti- and Au-contacted devices (see Figure S5 in Supporting Information). As presented in **Table 1**, the SBHs of aged WSe$_2$ were found to be 619, 575, 352, and 207 meV for In, Ti, Au, and Pd metal contacts, respectively. The SBHs were plotted to obtain pinning factors as shown in Figure 3d. The black line shows the pristine WSe$_2$ before O$_2$ plasma treatment with electron SBHs. The green line indicates the SBHs converted for hole according to the above Equation (1). The blue dashed line indicates the guideline for the perfectly de-pinned states for both electron and hole with respective values of 1 and −1. The pristine WSe$_2$ shows strong FLP. However, a decrease in the FLP from −0.06 to −0.36 was observed after aging the plasma-treated WSe$_2$ devices. It appears that the reduced FLP was observed after O$_2$ plasma treatment and subsequent aging of devices. Further, in the case of the Pd-contacted WSe$_2$ FET device, the extracted SBH for hole approached the Schottky–Mott limit approximately according to the blue-dashed guideline shown in Figure 3d. That is, the de-pinned behavior was confirmed in the case of the Pd-contacted device. The de-pinning property can also be confirmed by comparing the energy level of valence band maximum (VBM) and the work function of Pd. E_g of WSe$_2$ is 1.31 eV, and its affinity is 4.06 eV, so the energy level of VBM can reach 5.37 eV. The theoretical SBH can be confirmed in a simple manner by subtracting the energy level of VBM from the work function of Pd, which results in 0.25 eV. This value is similar to the SBH of Pd that we extracted, so it can be seen that de-pinning was eventually achieved by Pd contact.

Meanwhile, in the case of In contact, the extracted SBH values exhibit differences from the Schottky–Mott limit ($S = -1$) shown in the blue-dash guideline of Figure 3d, indicating that the FLP still exists in the case of the In contact. It is clear that the Pd and Au contacts with higher work function metals form a proper contact to these aged WSe$_2$ devices. As mentioned previously, the output characteristics of Pd and Au contact indicate a quasi-Ohmic behavior, in contrast to the Schottky contact behavior seen in the case of In and Ti contacts. Moreover, the field-effect mobility and R_c of Pd contact also resulted in 2 times higher mobility and 10 times reduced R_c compared to In contact, as shown in Figure S6 (Supporting Information).

To further investigate the transport properties, we analyzed tunneling characteristics in the following section by using the Fowler–Nordheim (F–N) tunneling and thermionic emission models.

2.3. Tunneling Behavior

The modulation of SBH results in a change in the transport behavior of the device, particularly in terms of tunneling across the MS contact. We investigated the carrier transport at the junction between aged WSe$_2$ and metal based on the F–N tunneling and thermionic emission models. The tunneling theory that originated from Simmons' theory[36] was represented by the following Equations (5) through (8).[37] The interpretation for direct tunneling can be obtained according to Equation (6), while that for F–N tunneling can be obtained according to Equation (8).

Direct Tunneling

$$I_D \propto V_D \exp\left[-\frac{4\pi d \sqrt{2m^* \phi_B}}{h}\right] \quad (5)$$

$$\ln\left(I_D / V_D^2\right) \propto \ln\left(1/V_D\right) - \frac{4\pi d \sqrt{2m^* \phi_B}}{h} \quad (6)$$

F–N Tunneling

$$I_D \propto V_D^2 \exp\left[-\frac{8\pi d \sqrt{2m^* \phi_B^3}}{3hqV_D}\right] \quad (7)$$

$$\ln\left(I_D / V_D^2\right) \propto -1/V_D \cdot \left(\frac{8\pi d \sqrt{2m^* \phi_B^3}}{3hq}\right) \quad (8)$$

Here, ϕ_B is the SBH, m^* is the effective mass, h is Planck's constant, and d is the width of the barrier. Tunneling transport can be analyzed according to the relationship between $\ln(I_D/V_D^2)$ and $\ln(1/V_D)$.[34,38,39] **Figure 4** shows the carrier transport results and the interpretation of the transport results for our aged WSe$_2$ devices. It can be seen that the above-mentioned tunneling Equations (6) and (8) are plotted as linear relationships of the logarithmic function in Figure 4a,b. That is, direct tunneling at the MS junction between aged WSe$_2$ and metals for Pd is inferred according to a linear relation, while F–N tunneling is used for forecasting for the In contact device. Figure 4c,d show the schematics of band alignment at the aged WSe$_2$–Pd/In junction. The reduced SBH and the de-pinned
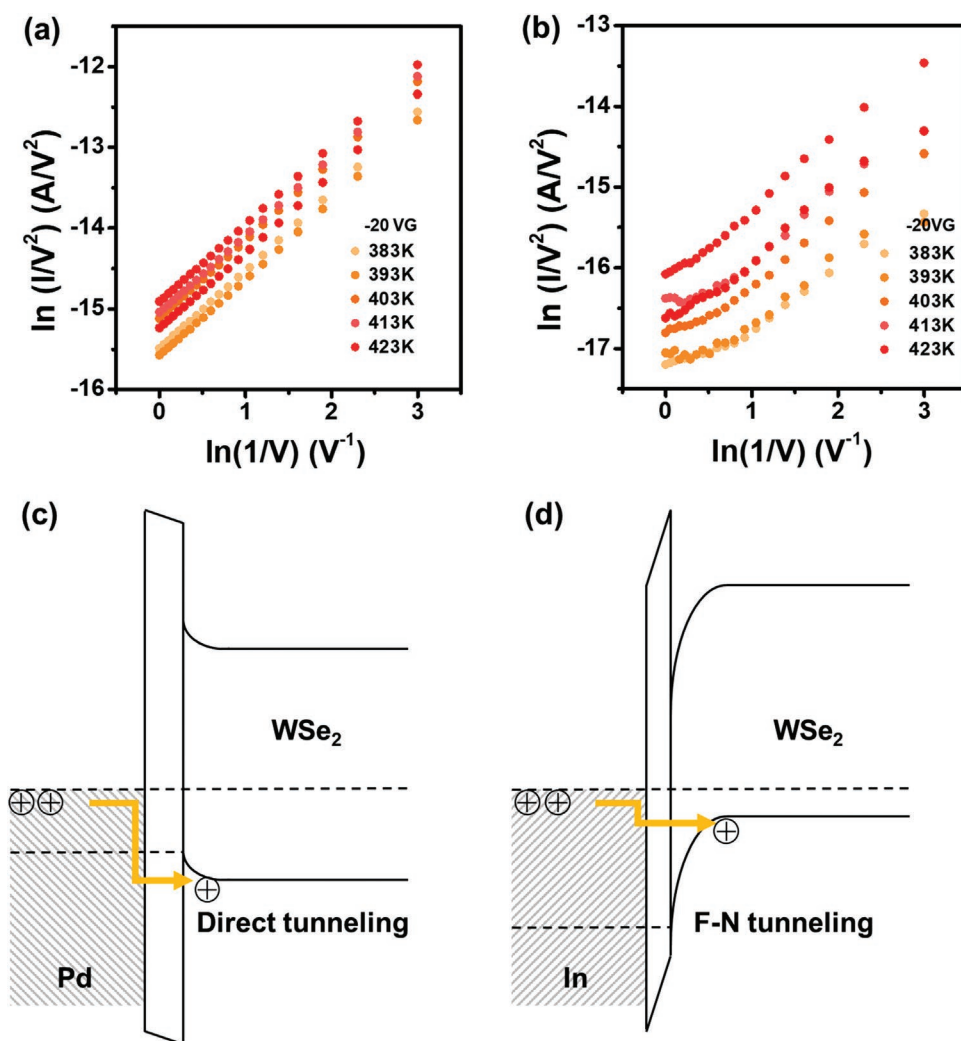
Figure 4. Carrier transport of aged WSe$_2$. a,b) F–N plots for Pd- and In-contacted aged devices, respectively. c,d) Band alignments of the MS junction for Pd- and In-contacted aged devices, respectively.

energy level of Pd-aged WSe$_2$ result in direct tunneling because of weak band bending, as shown in Figure 4c. However, F–N tunneling occurs in the case of In contact due to the strong band bending at the junction. Moreover, Ti contact as a low-work-function metal contact shows tunneling behavior that is similar to that of the In contact device. Ti contact shows instances of direct and F–N tunneling in the regions of low temperature and high temperature, respectively. By contrast, the direct tunneling occurs in the case of Au contact, similar to Pd contact. That is, the acceptor level becomes similar to the energy level of metals with a high work function, as p-doping due to O$_2$ plasma is performed in WSe$_2$. In the case of metal contact with a relatively high work function, band bending is weak, and direct tunneling occurs. Conversely, in the case of a metal contact with a low work function, FLP still occurs, and F–N tunneling is observed with the occurrence of substantial band bending.

Further, although the aging reduces the current level, we suggest a simple defect engineering process that is developed by protecting plasma-treated WSe$_2$ devices from degrading. The

degradation of doping occurs over time due to the interaction between the exposed surface of WSe$_2$ and the surrounding environment, such as moisture, contamination, etc. However, it is possible to prevent degradation by passivating the aged devices (see Figure S9, Supporting Information); that is, devices can be fabricated to have specific doping states by passivating the top surfaces of the devices. The passivation of devices by h-BN can prevent degradation from occurring by screening contamination from the environment at the surfaces of the devices.

3. Conclusion

WSe$_2$ FET devices were tested to assess the FLP induced by O$_2$ plasma treatment using contact metals of different work functions: In, Ti, Au, and Pd. The pinning factor changed from −0.06 for the pristine device to −0.36 for the aged devices. The changes in SBHs of Pd and Au were observed to be higher than those of In and Ti. Carrier transport was found to be influenced by the contact metals, e.g., for In and Ti, F–N and

direct tunneling occurred at the junction of metal–WO_x. This study demonstrates that industry-compatible O_2 plasma treatment can be efficiently used to improve carrier transport at the electrical contacts of 2D semiconductor devices by controlling FLP. Moreover, this work proposes a method for maintaining the aged WSe_2 FET behavior throughout the aging process, and it demonstrates the implementation of Fermi-level pinning-free devices with a more simplified process. It also demonstrates potential to realize a stable doping state by using the passivation effect of h-BN on the surface of O_2-plasma-treated and aged WSe_2 FET devices.

4. Experimental Section

Fabrication of Devices: WSe_2 was exfoliated on PDMS, after which WSe_2 was transferred onto SiO_2 (285 nm)/p^{++} Si substrate, which was then cleaned by sonication with acetone and IPA. To transfer WSe_2 onto the substrate, the substrate was heated up to 50 °C to achieve good attachment on the substrate. About 10 layered intrinsic WSe_2 flakes were used and they can be observed by an optical microscope, even on the PDMS substrate. WSe_2 was then coated by poly(methyl methacrylate) (PMMA) to conduct EBL. WSe_2 was patterned as a Hall-bar structure to confirm its reliable contact resistance via EBL. It was then etched in a plasma with the following conditions: a mixture gas of 10 sccm SF_6 and 30 sccm O_2, a working pressure of 30 mTorr, an inductively coupled plasma (ICP) power of 30 W, and an etching time of 90 s. Upon completion of the etching process, the remaining PMMA was removed by acetone, and it was coated again with PMMA to pattern the contact metal. Contact metals of 5 nm thick In, Ti, Au, and Pd were deposited onto each WSe_2 sample, and the contact metals were covered by 60 nm thick Au. Samples were first measured as pristine state, after which they were oxidized via O_2 plasma treatment with the following conditions: 200 s oxidation time, 30 W ICP power in 30 mTorr working pressure, and 30 sccm O_2 gas flow. Immediately following O_2 plasma treatment on WSe_2 devices, degenerately highly doped *I–V* behavior without the off-state appeared, but the off-state tended to emerge over time. Here, electrical measurements were performed. As those devices became stable, Schottky contact and Schottky barrier were formed. The devices were aged in vacuum until off-state appeared without encapsulation.

Contact Resistance Analysis: The contact resistance was calculated via the 4PP method by using Hall-bar structured devices in which the drain current was assumed to be constant at all locations flowing from source to drain. The voltage was measured drop by drop using two probes in the middles of the devices, and channel resistance was normalized by the length ratio of the distance of two inner probes with respect to the distance between source and drain.

Schottky Barrier Height Analysis: The aged WSe_2 devices were measured by varying temperature after they were aged, i.e., when off-state appeared in transfer curves. SBH was calculated by analyzing the drain current at various tested temperatures. The specific SBH values were extracted from the region where the slope changed compared to the threshold voltage region in the transfer curves. Moreover, SBHs of each metal (In, Ti, Au, and Pd) were extracted with flat-band voltages. Each energy level of SBHs of various contact metals was calculated by comparing the energy of valence/conduction band edges.

Tunneling Behavior Between Aged WSe_2 and Metal: Tunneling behavior was observed using the F–N emission model. Here, an F–N plot was prepared with the output curves of the devices.

Aging Properties of Aged WSe_2: Upon completion of the plasma treatment on WSe_2, the electrical performances of the devices were measured immediately. The devices were then aged in a desiccator in vacuum to prevent other molecules from reacting with air. The electrical properties, including 4PP measurement, were confirmed for each device after a vacuum aging process. Here, the vacuum aging process referred to a process in which the off-state in the transfer curve showed metallic

behavior right after the doping of WSe_2, which gradually decreased over time and showed semiconducting behavior demonstrating the off-state.

All measurements were conducted at a pressure of 20 mTorr, and the devices were characterized by an electrical analyzer (Agilent 4155C).

Supporting Information

Supporting Information is available from the Wiley Online Library or from the author.

Conflict of Interest

The authors declare no conflict of interest.

Data Availability Statement

The data that support the findings of this study are available from the corresponding author upon reasonable request.

[1] M. Zeng, Y. Xiao, J. Liu, K. Yang, L. Fu, *Chem. Rev.* **2018**, *118*, 6236.

[2] K. Khan, A. K. Tareen, M. Aslam, R. Wang, Y. Zhang, A. Mahmood, Z. Ouyang, H. Zhang, Z. Guo, *J. Mater. Chem. C* **2020**, *8*, 387.

[3] C. Huo, Z. Yan, X. Song, H. Zeng, *Sci. Bull.* **2015**, *60*, 1994.

[4] Q. Zhang, L. Mei, X. Cao, Y. Tang, Z. Zeng, *J. Mater. Chem. A* **2020**, *8*, 15417.

[5] H. Li, G. Lu, Y. Wang, Z. Yin, C. Cong, Q. He, L. Wang, F. Ding, T. Yu, H. Zhang, *Small* **2013**, *9*, 1974.

[6] H. Fang, S. Chuang, T. C. Chang, K. Takei, T. Takahashi, A. Javey, *Nano Lett.* **2012**, *12*, 3788.

[7] H. W. Guo, Z. Hu, Z. B. Liu, J. G. Tian, *Adv. Funct. Mater.* **2021**, *31*, 2007810.

[8] S. Manzeli, D. Ovchinnikov, D. Pasquier, O. v. Yazyev, A. Kis, *Nat. Rev. Mater.* **2017**, *2*, 17033.

[9] Z. Xu, H. Yang, X. Song, Y. Chen, H. Yang, M. Liu, Z. Huang, Q. Zhang, J. Sun, L. Liu, Y. Wang, *Nanotechnology* **2021**, *32*, 492001.

[10] C. S. Pang, T. Y. T. Hung, A. Khosravi, R. Addou, R. M. Wallace, Z. Chen, *IEEE Electron Device Lett.* **2020**, *41*, 1122.

[11] M. Yamamoto, S. Dutta, S. Aikawa, S. Nakaharai, K. Wakabayashi, M. S. Fuhrer, K. Ueno, K. Tsukagoshi, *Nano Lett.* **2015**, *15*, 2067.

ADVANCED
SCIENCE NEWS

www.advancedsciencenews.com

ADVANCED
ELECTRONIC
MATERIALS

www.advelectronicmat.de

[12] T. D. Ngo, M. Lee, Z. Yang, F. Ali, I. Moon, W. J. Yoo, *Adv. Electron. Mater.* **2020**, *6*, 2000616.

[13] N. R. Pradhan, D. Rhodes, S. Memaran, J. M. Poumirol, D. Smirnov, S. Talapatra, S. Feng, N. Perea-Lopez, A. L. Elias, M. Terrones, P. M. Ajayan, L. Balicas, *Sci. Rep.* **2015**, *5*, 8979.

[14] I. Moon, S. Lee, M. Lee, C. Kim, D. Seol, Y. Kim, K. H. Kim, G. Y. Yeom, J. T. Teherani, J. Hone, W. J. Yoo, *Nanoscale* **2019**, *11*, 17368.

[15] M. Yamamoto, S. Dutta, S. Aikawa, S. Nakaharai, K. Wakabayashi, M. S. Fuhrer, K. Ueno, K. Tsukagoshi, *Nano Lett.* **2015**, *15*, 2067.

[16] M. Yamamoto, S. Nakaharai, K. Ueno, K. Tsukagoshi, *Nano Lett.* **2016**, *16*, 2720.

[17] L. W. W. Fang, Z. Zhang, R. Zhao, J. Pan, M. Li, L. Shi, T. C. Chong, Y. C. Yeo, *J. Appl. Phys.* **2010**, *108*, 053708.

[18] A. Dimoulas, P. Tsipas, A. Sotiropoulos, E. K. Evangelou, *Appl. Phys. Lett.* **2006**, *89*, 252110.

[19] Y. H. Chen, C. Y. Cheng, S. Y. Chen, J. S. D. Rodriguez, H. T. Liao, K. Watanabe, T. Taniguchi, C. W. Chen, R. Sankar, F. C. Chou, H. C. Chiu, W. H. Wang, *npj 2D Mater. Appl.* **2019**, *3*, 49.

[20] Z. Yang, C. Kim, K. Y. Lee, M. Lee, S. Appalakondaiah, C. H. Ra, K. Watanabe, T. Taniguchi, K. Cho, E. Hwang, J. Hone, W. J. Yoo, *Adv. Mater.* **2019**, *31*, 1808231.

[21] R. S. Chen, G. Ding, Y. Zhou, S. T. Han, *J. Mater. Chem. C* **2021**, *9*, 11407.

[22] C. Kim, I. Moon, D. Lee, M. S. Choi, F. Ahmed, S. Nam, Y. Cho, H. J. Shin, S. Park, W. J. Yoo, *ACS Nano* **2017**, *11*, 1588.

[23] X. Liu, D. Qu, L. Wang, M. Huang, Y. Yuan, P. Chen, Y. Qu, J. Sun, W. J. Yoo, *Adv. Funct. Mater.* **2020**, *30*, 2004880.

[24] P. R. Pudasaini, A. Oyedele, C. Zhang, M. G. Stanford, N. Cross, A. T. Wong, A. N. Hoffman, K. Xiao, G. Duscher, D. G. Mandrus, T. Z. Ward, P. D. Rack, *Nano Res.* **2018**, *11*, 722.

[25] D. Qu, X. Liu, M. Huang, C. Lee, F. Ahmed, H. Kim, R. S. Ruoff, J. Hone, W. J. Yoo, *Adv. Mater.* **2017**, *29*, 1606433.

[26] M. S. Choi, M. Lee, T. D. Ngo, J. Hone, W. J. Yoo, *Adv. Electron. Mater.* **2021**, *7*, 2100449.

[27] W. Liu, J. Kang, D. Sarkar, Y. Khatami, D. Jena, K. Banerjee, *Nano Lett.* **2013**, *13*, 1983.

[28] Y. Wang, J. C. Kim, R. J. Wu, J. Martinez, X. Song, J. Yang, F. Zhao, A. Mkhoyan, H. Y. Jeong, M. Chhowalla, *Nature* **2019**, *568*, 70.

[29] C. M. Smyth, L. A. Walsh, P. Bolshakov, M. Catalano, R. Addou, L. Wang, J. Kim, M. J. Kim, C. D. Young, C. L. Hinkle, R. M. Wallace, *ACS Appl. Nano Mater.* **2019**, *2*, 75.

[30] C. S. Pang, T. Y. T. Hung, A. Khosravi, R. Addou, Q. Wang, M. J. Kim, R. M. Wallace, Z. Chen, *Adv. Electron. Mater.* **2020**, *6*, 1901304.

[31] B. Ofuonye, J. Lee, M. Yan, C. Sun, J. M. Zuo, I. Adesida, *Semicond. Sci. Technol.* **2014**, *29*, 095005.

[32] A. Anwar, B. Nabet, J. Culp, F. Castro, *J. Appl. Phys.* **1999**, *85*, 2663.

[33] I. Dökme, *Microelectron. Reliab.* **2011**, *51*, 360.

[34] J. Appenzeller, M. Radosavljević, J. Knoch, P. Avouris, *Phys. Rev. Lett.* **2004**, *92*, 4.

[35] K. Kim, S. Larentis, B. Fallahazad, K. Lee, J. Xue, D. C. Dillen, C. M. Corbet, E. Tutuc, *ACS Nano* **2015**, *9*, 4527.

[36] J. G. Simmons, *J. Appl. Phys.* **1963**, *34*, 1793.

[37] F. Ahmed, M. S. Choi, X. Liu, W. J. Yoo, *Nanoscale* **2015**, *7*, 9222.

[38] J. M. Beebe, B. Kim, J. W. Gadzuk, C. D. Frisbie, J. G. Kushmerick, *Phys. Rev. Lett.* **2006**, *97*, 026801.

[39] B. K. Sarker, S. I. Khondaker, *ACS Nano* **2012**, *6*, 4993.